

# Probing the biophysical interplay between a viral genome and its capsid

J. Snijder<sup>1,2,3</sup>, C. Uetrecht<sup>1,2†</sup>, R. J. Rose<sup>1,2</sup>, R. Sanchez-Eugenía<sup>4</sup>, G. A. Martí<sup>5</sup>, J. Agirre<sup>4,6</sup>,  
D. M. A. Guérin<sup>4,6</sup>, G. J. L. Wuite<sup>3</sup>, A. J. R. Heck<sup>1,2\*</sup> and W. H. Roos<sup>3\*</sup>

**The interaction between a viral capsid and its genome governs crucial steps in the life cycle of a virus, such as assembly and genome uncoating. Tuning cargo-capsid interactions is also essential for successful design and cargo delivery in engineered viral systems. Here we investigate the interplay between cargo and capsid for the picorna-like *Triatoma* virus using a combined native mass spectrometry and atomic force microscopy approach. We propose a topology and assembly model in which heterotrimeric pentons that consist of five copies of structural proteins VP1, VP2 and VP3 are the free principal units of assembly. The interpenton contacts are established primarily by VP2. The dual role of the genome is first to stabilize the densely packed virion and, on an increase in pH, second to trigger uncoating by relaxing the stabilizing interactions with the capsid. Uncoating occurs through a labile intermediate state of the virion that reversibly disassembles into pentons with the concomitant release of protein VP4.**

In addition to coding for viral genes, the genome of a virus plays an essential role through its interactions with the viral capsid. For example, the genome often facilitates capsid assembly and, once packaged, the genome stabilizes and reinforces the virus<sup>1</sup>. This interplay between the capsid and its cargo is therefore a crucial factor in designing engineered viral systems<sup>2</sup>. An increased knowledge of genome-capsid interactions can enhance our understanding of viruses in their role as pathogens, drug-delivery vehicles and nanotechnological platforms. However, details of genome release (that is, uncoating) and virion assembly are not easily accessible experimentally because of the heterogeneity and transient nature of several co-occurring intermediate states. Most analytical and biochemical assays are unable to resolve these small subpopulations. The study of virus assembly and uncoating thus requires techniques that are capable of simultaneous detailed structural and physical characterization of components in complex mixtures.

In recent years, both native mass spectrometry (MS) and atomic force microscopy (AFM) have emerged as alternative, powerful platforms for the study of viruses<sup>3–6</sup>. Where more-established structural biology techniques suffer, these alternatives effectively capture assembly intermediates, and so expose details of viral assembly and maturation pathways. Key to these techniques is the high mass selectivity of MS and the single-particle approach of AFM. We previously implemented ion-mobility spectrometry (IMS) to characterize the geometry of *in vitro* reconstituted capsid assembly intermediates<sup>7</sup>. We demonstrate here that the combination of this IMS methodology with tandem MS analysis yields very rich structural information on authentic virions, their genome-free capsid counterparts and the assembly intermediates. Essential aspects of the structural model are confirmed and further examined by high-resolution AFM imaging. Additionally, we apply AFM in its

force-spectroscopy mode to characterize in detail the process of genome uncoating.

With this powerful combination of native MS and AFM, we studied the picorna-like *Triatoma* virus (TrV). The single-stranded ribonucleic acid (ssRNA) insect virus TrV is a member of the Dicistroviridae family and is closely related to common human pathogens such as poliovirus<sup>8</sup>. Infection is lethal to the insect host of TrV, *Triatoma infestans*<sup>9,10</sup>. As these triatomine insects are the most important vectors for Chagas disease<sup>11</sup>, recently recognized by the World Health Organization (WHO) as one of several neglected tropical diseases that places considerable strain on public health in affected regions, TrV has potential applications as a biopesticide<sup>10</sup>. TrV consists of a 9,010 nucleotide positive-sense ssRNA genome that is encapsidated by 60 copies of the structural proteins VP2, VP4, VP3 and VP1 (from the N-terminus to the C-terminus on the precursor P1)<sup>8,12,13</sup>. VP1/2/3 are the main structural proteins of the capsid (Protein Data Bank (PDB) code, 3NAP), whereas the role of VP4 is currently unclear<sup>14</sup>. The capsid proteins VP1/2/3 have a jelly-roll fold, typical of picorna(-like) viruses, and a high degree of structural homology to the related cricket paralysis virus<sup>15</sup>. Five copies of the VP1/2/3 heterotrimer are arranged in five-fold symmetric substructures (capsomers, called ‘pentons’), 12 of which form the fully closed capsid. VP1 is centred on the five-fold icosahedral symmetry axis and protrudes out from the capsid surface. VP2 and VP3 are situated on quasi-three-fold and two-fold related symmetry axes, whereby VP2 establishes interpenton contacts via a domain-swapping interaction between capsomers.

The insect host of TrV feeds on blood and is adapted to cope with the toxic effects of haem by maintaining acidic pH in the midgut<sup>16–19</sup>. In contrast to the acidic conditions in the midgut of *T. infestans*, the hindgut is maintained at alkaline pH<sup>17,20</sup>. As TrV infection takes place via an oral-faecal route, large pH changes

<sup>1</sup>Biomolecular Mass Spectrometry and Proteomics, Bijvoet Center for Biomolecular Research and Utrecht Institute for Pharmaceutical Sciences, Utrecht University, Padualaan 8, 3584 CH, Utrecht, The Netherlands, <sup>2</sup>Netherlands Proteomics Centre, Padualaan 8, 3584 CH, Utrecht, The Netherlands, <sup>3</sup>Natuur-en Sterrenkunde and LaserLab, Vrije Universiteit, De Boelelaan 1081, Amsterdam, The Netherlands, <sup>4</sup>Unidad de Biofísica (CSIC, UPV-EHU) Barrio Sarriena S/N, 48940 Leioa, Bizkaia, Spain, <sup>5</sup>Centro de Estudios Parasitológicos y de Vectores (CEPAVE-CCT-La Plata-CONICET-UNLP), 2#584 (1900) La Plata, Argentina, <sup>6</sup>Fundación Biofísica Bizkaia. Barrio Sarriena S/N, 48940 Leioa, Bizkaia, Spain; <sup>†</sup>Present address: Sample Environment Group, European XFEL GmbH, Notkestrasse 85, 22607 Hamburg, Germany and Laboratory of Molecular Biophysics, Department of Cell and Molecular Biology, Uppsala University, Husargatan 3, 75124 Uppsala, Sweden. \*e-mail: wroos@few.vu.nl; a.j.r.heck@uu.nl

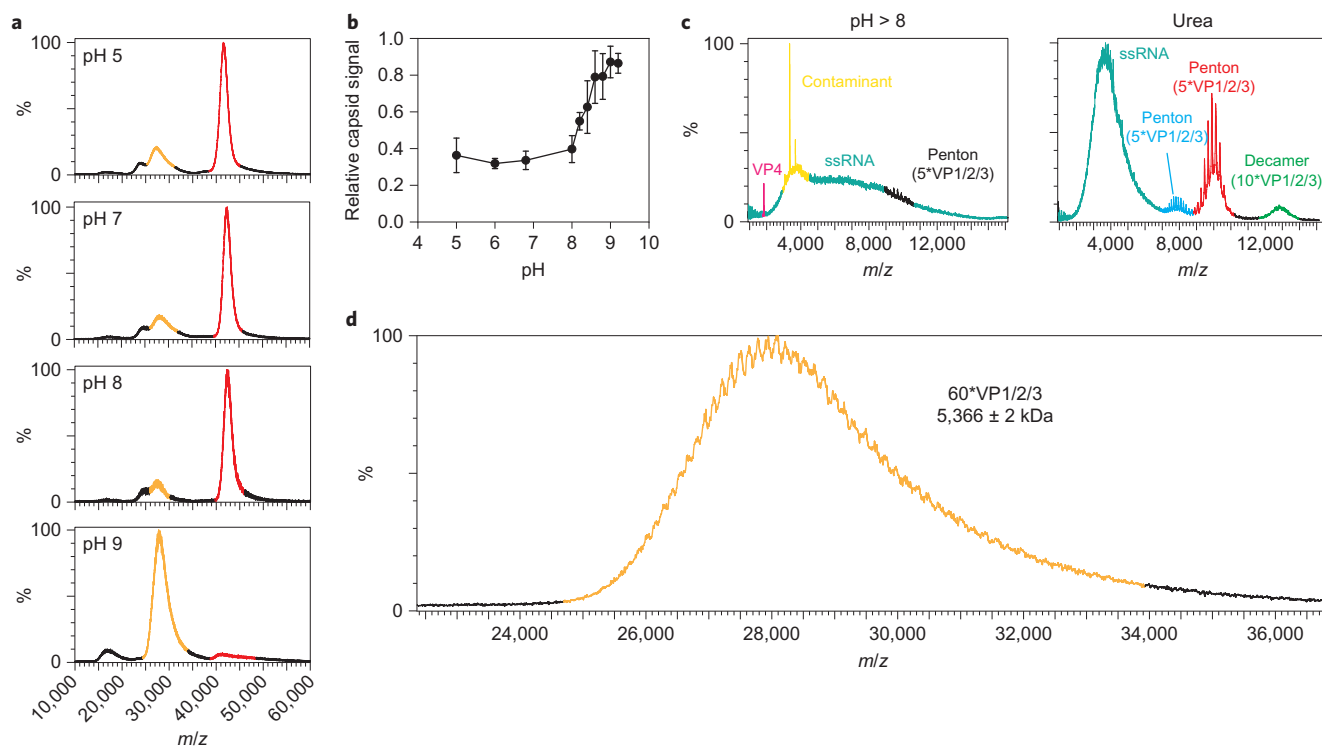


**Figure 1 | Alkaline-triggered uncoating of TrV monitored by native MS. a**, Spectra of TrV virions at different pH values. The signal that corresponds to virion is highlighted in red ( $m/z \sim 40,000$ ,  $M_w \sim 8.3$  MDa) and that to empty capsids is highlighted in yellow ( $m/z \sim 28,000$ ,  $M_w \sim 5.4$  MDa). The shoulder on the capsid peak at pH 5–7, which shifts towards lower  $m/z$  at high pH, is not an ‘authentic’ ion signal, but a time-of-flight related artefact that arises for high-mass complexes. It relates to the real signals of virion and capsid, respectively. **b**, Relative amount of capsid versus virion signal as a function of pH. Data points are the average of triplicate experiments and error bars represent s.d. **c**, Species detected at lower  $m/z$  are associated with alkaline-triggered uncoating or denaturation. Ions (indicated by the colour coding) that originate from RNA, VP4 and pentons were detected (left). Pentons and penton dimers were also the main disassembly products of urea-induced denatured virions (right). The additional charge-state distribution of pentons in urea is indicative of unfolding. **d**, Mass spectrum of the r-empty capsid, with an elevated collision voltage (180–200 V) enhancing desolvation.

1 may play an important role in infectivity<sup>21</sup>. Here we assess assembly,  
 2 stability and genome release in TrV as a function of pH. We deter-  
 3 mine the mass of the intact TrV virion and capsid with unprece-  
 4 dented precision and, using naturally occurring infectious  
 5 particles, we uncover an *in vitro* pathway of alkaline-triggered  
 6 uncoating. We show how this pathway is regulated by genome-  
 7 capsid interactions and we present a model of the dual role of the  
 8 genome in capsid stabilization and genome uncoating.

## 9 Results

10 **A pathway of alkaline-triggered genome release.** We tested the pH  
 11 stability of TrV using native MS. The theoretical (as predicted from  
 12 the sequence) and experimentally measured masses of the  
 13 individual VPs and the assemblies detected by MS are given in  
 14 Supplementary Table S1. Figure 1a shows native mass spectra of  
 15 purified TrV virions at pH 5, 7, 8 and 9. As well as the full  
 16 genome-packed virions, the extracted samples contain a small  
 17 amount of naturally occurring empty capsids (n-empty) that are  
 18 thought to arise from misprocessing of P1. This misprocessing,  
 19 which is predominantly inefficient cleavage of VP0 into VP3/4  
 20 (ref. 14), and the absence of RNA in n-empty capsids are the  
 21 main differences between this capsid particle and the virion.  
 22 Using MS, the n-empty capsids ( $\sim 5.4$  MDa) can be well separated  
 23 from the full virions ( $\sim 8.3$  MDa). The MS data reveal that,  
 24 whereas TrV is acid stable, alkaline conditions do trigger release  
 25 of the genome, as can be seen from the loss of virion signal. The  
 26 transition from virion to empty capsid occurs predominantly  
 27 between pH 8 and pH 9 (Fig. 1b).

28 In the low  $m/z$  range of a virion sample at pH > 8, several dis-  
 29 assembly products were detected (Fig. 1c). The unresolved high

baseline signals in these spectra originate from degradation products 30  
 of the ssRNA genome, as validated by tandem MS (Supplementary 31  
 Fig. S1). Additional peaks were observed that originated from the 32  
 VP4 protein. The samples also contained a 36 kDa contaminant 33  
 that was already present under neutral conditions and therefore 34  
 not related to genome release (Supplementary Fig. S2). Finally, 35  
 several peaks that belong to free pentons ( $5^*VP1/2/3$ ) were 36  
 detected. We hypothesized that the pentons are assembly interme- 37  
 diates that originate from disassembled virions, but subsequently 38  
 reassemble into empty capsids (denoted as ‘r-empty capsid’ to dis- 39  
 tinguish them from the n-empty capsids). Recently, for the related 40  
 bovine enterovirus it was demonstrated that pentons of VP proteins 41  
 can assemble into empty capsids under conditions of high ionic 42  
 strength<sup>22</sup>. We confirmed that pentons of TrV are, indeed, assembly 43  
 intermediates of empty capsids by demonstrating that the alkaline- 44  
 triggered uncoating reaction yields more free penton under con- 45  
 ditions of low ionic strength and that these pentons assemble 46  
 into empty capsids when the ionic strength is increased sub- 47  
 sequently (see Supplementary Fig. S3). These results indicate that 48  
 alkaline-triggered genome release occurs through reversible disas- 49  
 sembly of the virion into pentons and is accompanied by release of 50  
 VP4. Pentons are also formed, as well as some dimers of pentons, 51  
 after denaturation of the virion in 8 M urea. This confirms that the 52  
 penton is a fundamental and very stable structural unit of the 53  
 capsid. In contrast to the alkaline-induced pentons, urea-denatured 54  
 penton subcomplexes are no longer assembly competent, as no 55  
 intact capsid is detected after the removal of urea (Supplementary 56  
 Fig. S4). The presence of disassembly products in high pH and after 57  
 denaturation in urea was further confirmed using native polyacryl- 58  
 amide gel electrophoresis (PAGE; Supplementary Fig. S5). 59

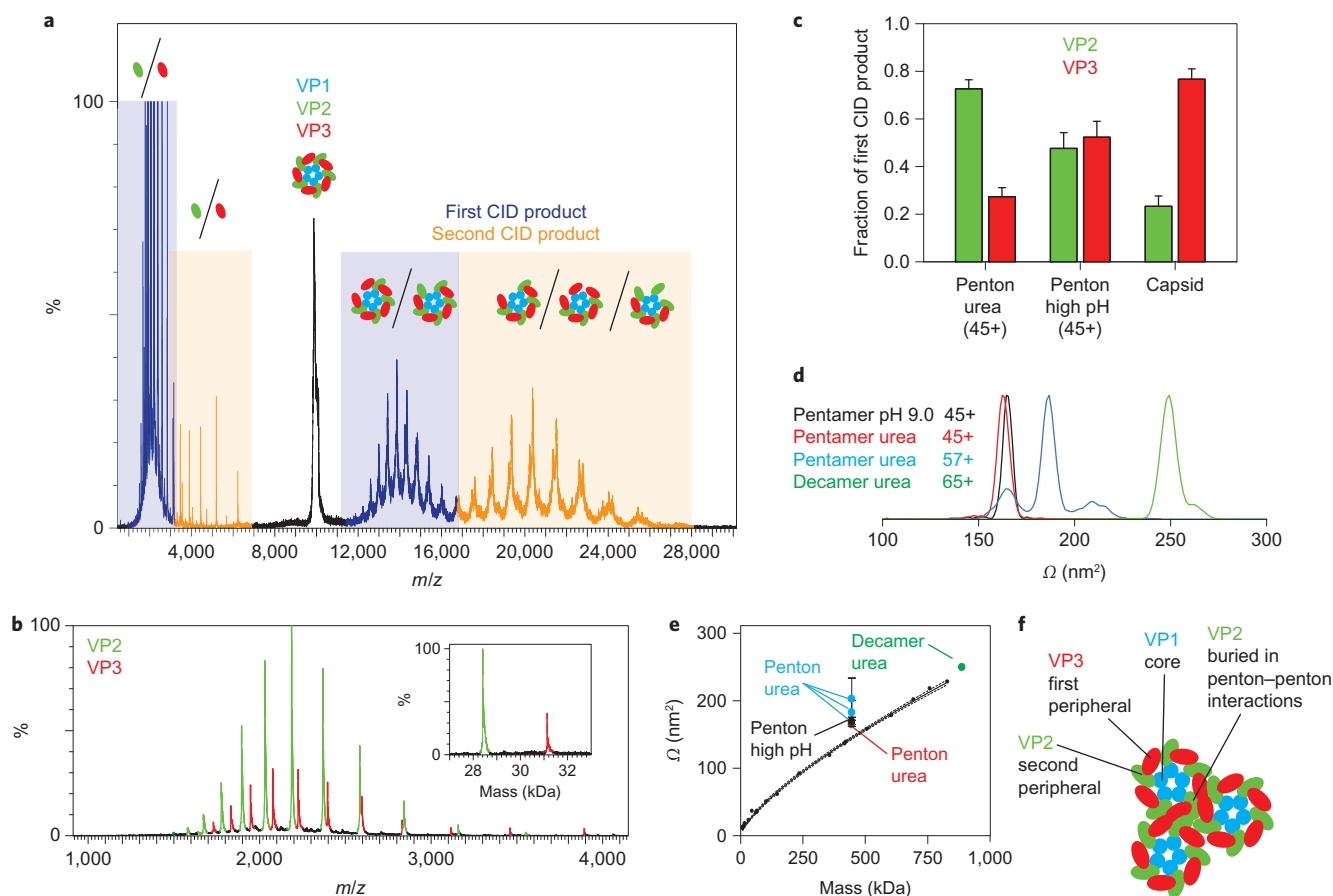


**Figure 2 | Native MS-based topology model of TrV. a**, Tandem MS spectrum of a denatured penton at a 160 V collision voltage that shows the sequential loss of two subunits. **b**, Enlargement of the ejected subunits from the denatured pentons. The first CID product consists solely of VP2 and VP3, which shows that VP1 is a core subunit, but VP2 and VP3 are peripheral. The relative amounts of each subunit are estimated from integrated peak areas, as shown in the inset. **c**, Relative amounts of dissociated VPs from the indicated complexes. The selected charge state is indicated in parentheses. Data are averages from triplicate experiments and error bars represent s.d. Urea-induced pentons preferentially eliminate VP2 under CID, and the r-empty capsids lose VP3 more easily. **d**, Collision cross-section ( $\Omega$ ) profiles extracted from the ion-mobility MS data of pentons and penton dimers. **e**, Plot of  $\Omega$  versus molecular mass for a range of protein complexes analysed under identical conditions by IMS. Solid black circles represent globular proteins and protein complexes. The black line is a power function fitted to these points ( $\Omega = 2.41 \times \text{mass}^{0.67}$ ,  $R^2 = 0.99$ ). TrV pentons and penton dimers are plotted as averages from triplicate experiments and error bars represent 2 s.d. The pentons fall significantly outside the confidence interval for globular complexes, which suggests that they have retained a sheet-like structure. **f**, MS-based topology model of TrV. Penton-assembly intermediates are composed of five copies of VP1/2/3. VP1 is the core subunit oriented along the five-fold icosahedral symmetry axis. VP2 and VP3 are peripheral subunits. VP2 is the main anchor for assembly and is buried in penton-penton contacts.

1 Raising the MS collision voltage (180–200 V using xenon as the  
 2 collision gas) enhances desolvation<sup>23</sup> and here resulted in a clearly  
 3 resolved series of charge states for the r-empty capsid (Fig. 1d),  
 4 which allowed a precise mass determination of  $5,366 \pm 2$  kDa.  
 5 This is in good agreement with a calculated mass for  $60 \times \text{VP1}/2/3$   
 6 (the experimental mass deviates from the theoretical by +0.1%,  
 7 probably because of incomplete desolvation and residual binding  
 8 of small molecules and counterions). The analysis is also highly  
 9 reproducible as five replicate analyses resulted in an average mass  
 10 of  $5,362 \pm 2$  kDa. This provides direct evidence that reassembly is  
 11 complete, albeit without the incorporation of RNA or VP4. The  
 12 mass assignment and exact stoichiometry of the r-empty capsids  
 13 was confirmed further with tandem MS at a higher collision  
 14 voltage (260 V) (Supplementary Fig. S6).

15 We observed no differences in peak position of the n-empty  
 16 capsid and remaining virion with an increase in pH (virion peak  
 17  $41,700 \pm 140$   $m/z$  at pH 6.8 and  $41,600 \pm 130$   $m/z$  at pH 9.0;  
 18 n-empty capsid  $29,420 \pm 260$   $m/z$  at pH 6.8 and  $29,710 \pm 200$   $m/z$   
 19 at pH 9.0) and no detectable disassembly products of the n-empty  
 20 capsids at pH 9 (Fig. 1a and Supplementary Fig. S7). There was

also no significant change in the autofluorescence of the capsid proteins at elevated pH (Supplementary Fig. S8). Therefore, no conformational changes to the effect of a different chargeable surface area or changes in the vicinity of aromatic residues accompany genome release. Thus, alkaline-triggered uncoating in TrV is caused uniquely by the presence of the ssRNA. We also calculated the binding energies between VP1/2/3 protomers within and between pentons at pH 7 and pH 9 as modelled in the crystal structure of TrV (Supplementary Fig. S9). The intramolecular interactions were stronger within a penton than between pentons and there were no substantial changes with increasing pH. This both explains the occurrence of the penton as a fundamental structural unit of the capsid and confirms a unique role for the ssRNA in alkaline-triggered uncoating.

**MS-based topology models of TrV.** With collision-induced dissociation (CID) and IMS of protein complexes, topology models can be reconstructed, even of low-abundance components in complex mixtures<sup>24,25</sup>. In CID, peripheral subunits tend to dissociate more readily than core subunits. Thus, by carefully

1 examining the dissociation behaviour of selected protein complexes  
2 during tandem MS, subunit locations can be determined. A tandem  
3 mass spectrum of individual TrV pentons is shown in Fig. 2a and  
4 reveals the sequential loss of two monomeric subunits after  
5 activation with CID. Figure 2b shows an enlargement of the ejected  
6 subunits during the first CID event. There is no detectible  
7 elimination of VP1, which suggests VP1 is a core subunit, whereas  
8 the facile elimination of VP2 and VP3 indicates that they are  
9 situated more towards the periphery of the penton.

10 The relative amount of dissociated VP2 and VP3 can be deter-  
11 mined by integrating the ion intensities over all their respective  
12 charge states (Fig. 2c). We performed CID on the pentons formed  
13 by either alkaline treatment or urea treatment, and on the intact  
14 r-empty capsids. The assembly-competent pentons, generated by  
15 alkaline-triggered uncoating, revealed no preferential dissociation  
16 of either VP2 or VP3. In the r-empty capsids, we observed substan-  
17 tially less elimination of VP2 compared to that of VP3, which indi-  
18 cates that VP2 is buried more deeply and stabilized by interpenton  
19 contacts. The assembly-incompetent denatured pentons show the  
20 opposite trend. VP2 is preferentially eliminated, which indicates  
21 diminished contacts or partial unfolding of the subunit. Therefore  
22 our CID data reveal the central role of VP2 for the assembly of  
23 the TrV capsid.

24 Using IMS, a coarse geometry of protein assemblies can be deter-  
25 mined and conformational substates can be distinguished by deter-  
26 mining a rotationally averaged collisional cross-section ( $\Omega$ )<sup>25</sup>. It was  
27 shown previously that IMS can be used to distinguish between  
28 sheet-like and globular structures of viral assembly intermediates  
29 by observing how cross-sections scale with molecular mass<sup>7,26</sup>. We  
30 performed travelling-wave IMS on subcomplexes of TrV to deter-  
31 mine the geometry of the assemblies (Fig. 2d and Supplementary  
32 Table S2). Pentons with lower charges and penton dimers showed  
33 narrow peaks, which indicates folded and homogeneous conforma-  
34 tions. Denatured pentons of higher charge displayed multiple  
35 larger conformations, consistent with their more unfolded nature.  
36 Comparison of the obtained cross-sections of the pentons with  
37 those from a large set of globular proteins shows that the pentons  
38 are significantly larger than globular proteins of equal molecular  
39 mass (Fig. 2e). This is indicative of sheet-like (that is, capsomer)  
40 structures. Whereas pentons appear as capsomer structures, the  
41 denatured penton dimers follow more closely the same trend as  
42 globular proteins. This suggests that penton dimers hinge on the  
43 penton–penton interface and collapse into a less-extended structure  
44 (Supplementary Fig. S10).

45 The combined CID and IMS analysis of TrV results in the top-  
46 ology model presented in Fig. 2f. Assembly intermediates of TrV  
47 are five-fold symmetric structures with VP1 located at the core  
48 around the symmetry axis. VP2 and VP3 are located at the periph-  
49 ery of the complex. VP2 is the main anchor for establishing inter-  
50 penton contacts and is crucial for the assembly of complete capsids.

51 **Mechanical properties of TrV reveal the mechanism of pH-**  
52 **triggered uncoating.** To probe the capsid–genome interplay  
53 further, the elastic strength and mechanical resilience of TrV  
54 capsid and virion were studied using AFM nanoindentation.  
55 With this approach, it has been demonstrated that genome  
56 packaging has a stabilizing effect on the capsids of a diverse set of  
57 viruses<sup>27–29</sup>. Our results described above indicate that the ssRNA  
58 triggers disassembly of the TrV capsid under alkaline conditions,  
59 which results in release of the genome. Therefore, TrV was  
60 probed with AFM nanoindentation in the pH range 7–9 to see  
61 whether there was a mechanical basis for alkaline-triggered  
62 uncoating. A typical force–distance curve (FDC) of TrV can be  
63 divided into three stages (Fig. 3a). After imaging, the tip of the  
64 cantilever is positioned over the centre of the particle and pushed  
65 into the capsid. There is zero force with  $z$ -displacement until the

tip and sample make contact. As the tip pushes down on the  
particle, there is a linear increase in force from which the spring  
constant  $k$  of the particle is determined. A higher load results in  
mechanical failure. This can be seen from a sharp transition in  
the FDC that is referred to as the breaking force,  $F_{\text{break}}$ .

TrV virions and n-empty capsids appeared as spherical particles  
of  $\sim 33$  nm in AFM imaging (Fig. 3b and Supplementary Table S3).  
The five-fold protrusions of VP1 can be distinguished on the capsid  
surface<sup>30</sup>. Imaging after nanoindentation revealed that mechanical  
failure of TrV resulted in capsid disassembly, similar to force-  
induced disassembly of the minute virus of mice<sup>31</sup>. Instead of a  
visible capsid, there were now up to 12 smaller particles. On  
closer inspection, each of these smaller breakdown products con-  
sisted of five smaller subunits arranged in a five-fold rotation. The  
dimensions of these particles are strikingly similar to those of  
pentons of 5\*VP1/2/3 (Supplementary Table S4). This indicates  
that pentons are the mechanical building blocks of TrV. Similar  
particles could be observed in AFM images of the virion at pH 9  
before nanoindentation, which indicates both that pentons are  
assembly intermediates for alkaline-triggered uncoating and  
that they retain the capsid-like capsomer structure in isolation,  
confirming our ion-mobility findings (Supplementary Fig. S11  
and Supplementary Table S4).

At neutral pH, virions are both stiffer (higher  $k$ ) and more resi-  
lient to higher forces than are empty capsids (Fig. 3c.). Moving  
towards increasingly alkaline conditions the mechanical response  
of the virion shifts towards that of the empty capsid via a discrete  
intermediate state (Fig. 3d). The intermediate state is most popu-  
lated at pH 8. From our MS analyses described above, we know  
that this intermediate still encloses the genome (Fig. 1a). The inter-  
mediate is characterized mechanically by a spring constant equal to  
that of the empty capsid, and a breaking force similar to that of the  
intact virion. Mechanically, the r-empty capsids that arise from alka-  
line-triggered uncoating are indistinguishable from n-empty capsids  
at pH 9. The mechanical properties of virions, the uncoating inter-  
mediate and empty capsids are given in Supplementary Table S5.  
The transition from virion to intermediate can be reversed by low-  
ering the pH back to neutral; the transition from virion/intermedi-  
ate to r-empty capsid is irreversible (Supplementary Fig. S12). As  
with the n-empty capsid, the mechanical response of the r-empty  
capsid at pH 7 is equal to that at pH 9. As an additional check  
that reassembly takes place, we assessed the particle density of  
TrV on the AFM substrate, and showed that it is equal at all pHs  
(Supplementary Fig. S13).

The material properties of icosahedral capsids can be approxi-  
mated within the framework of continuum thin-shell theory<sup>5</sup>.  
Here, the spring constant  $k$  of a shell with radius  $R$  and thickness  
 $h$  is related uniquely to the Young's modulus  $E$  of the capsid  
material, following  $k = \alpha Eh^2/R$ , where  $\alpha$  is a proportionality  
factor that is typically close to 1. The spring constant of r-empty  
capsids is on average  $0.43 \text{ N m}^{-1}$  and the average shell radius and  
thickness as described in the crystal structure of TrV (PDB code,  
3NAP) are 13.4 and 3.4 nm, respectively. These values yield a  
Young's modulus of  $E = 0.54 \text{ GPa}$  for the empty capsids. We  
know that the elasticity of the capsid is unaltered by alkaline pH  
and the measured particle height is also unaltered (this was con-  
firmed additionally by IMS of the intact capsids and virion,  
Supplementary Table S6). Hence, continuum thin-shell theory  
suggests that the increased spring constant of the virion results  
from an effective increase in shell thickness. With a spring constant  
of  $1.46 \text{ N m}^{-1}$ , the shell thickness of the virion is estimated at  
6.0 nm, that is, a genome-induced effective increase of 2.6 nm com-  
pared to that of r-empty capsids.

Dicistroviruses package an enormous amount of genomic  
material compared to other ssRNA viruses, such as the bromo-  
viruses<sup>1</sup>. TrV packages have over 9 kb of ssRNA compared to just

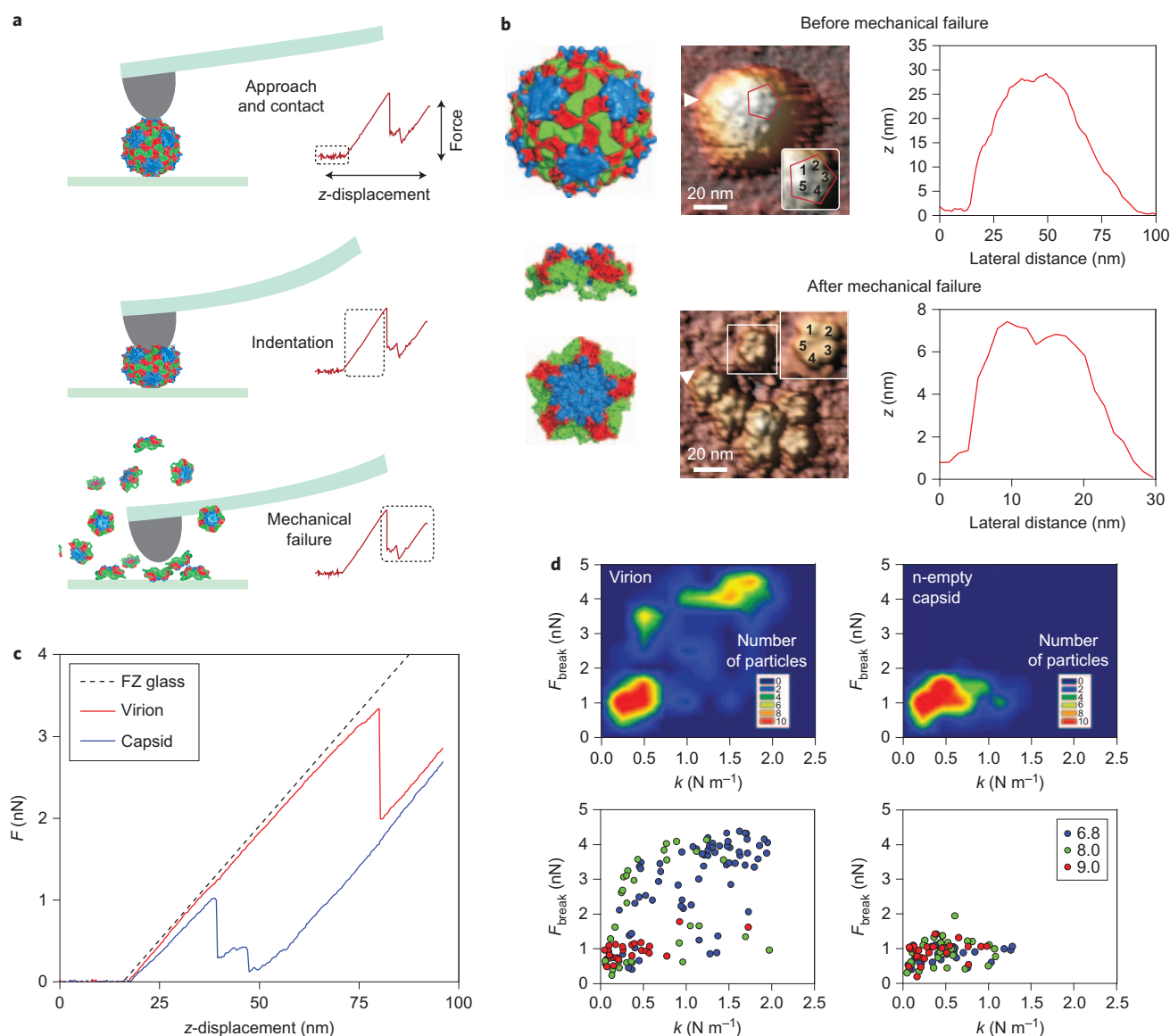


**Figure 3 | A mechanical basis for alkaline-triggered uncoating of TrV.** **a**, Schematic of AFM nanoindentation. **b**, Before nanoindentation, TrV appears as round particles of ~33 nm. Surface protrusions of VP1 are also visible (left). Surface renderings of intact capsids and pentons are shown for reference, with VP1 in blue, VP2 in green and VP3 in red (PDB code, 3NAP). Mechanical failure results in complete disassembly into pentons (centre). The corresponding height profiles are taken along the line of the white arrowheads (right). **c**, FDCs of virion and n-empty capsids at neutral pH. **d**, The bottom panels show the individual points at pH 6.8, pH 8 and pH 9, from which the two-dimensional density distributions ( $k$  versus  $F_{\text{break}}$ ) of single virions (left top panel) versus n-empty capsids (right top panel) were calculated. The virion under neutral pH has a characteristically higher spring constant and breaking force than the empty capsid. With increasing pH, the spring constant decreases but the high breaking force is maintained, which results in a discrete intermediate state. Consistent with genome release to yield empty capsids, all the particles are mechanically indistinguishable from n-empty capsids at pH 9.

1 3 kb in cowpea chlorotic mottle virus, but they both have a compar- 16  
 2 able diameter of ~30 nm. The packing density in TrV is even higher 17  
 3 than that in bacteriophage  $\lambda$ , which is thought to possess a high 18  
 4 internal pressure of several tens of atmospheres because of the high 19  
 5 density of double-stranded deoxyribonuclease it encapsidates 20  
 6 (based on the internal volumes and number of nucleotides/base 21  
 7 pairs, the charge densities compare as  $-1.03$  versus  $-1.34$  electrons 22  
 8  $\text{nm}^{-3}$  in bacteriophage  $\lambda$  and TrV, respectively; see Supplementary 23  
 9 Information). Confining such a large molecule to the relatively small 24  
 10 inner volume of the capsid is bound to have a high energetic cost, 25  
 11 which requires, for instance, significant dehydration of the 26  
 12 ssRNA<sup>32</sup>. Furthermore, the observation of polyamines in picorna- 27  
 13 viruses suggests that condensation of the genome onto counterions 28  
 14 is required to facilitate genome packaging<sup>33</sup>. The effective strength- 29  
 15 ening of the virion at neutral pH is probably the result of a 30

combination of nonspecific interactions of the RNA with positive 16  
 patches on the inner capsid wall and condensation of the RNA by 17  
 counterions, which confines the densely packed RNA to the inner 18  
 capsid volume. We confirmed that there is an electrostatic compo- 19  
 nent that determines the higher spring constant of the virion 20  
 compared with that of empty capsids by testing the response to 21  
 nanoindentation in high concentrations of  $\text{MgCl}_2$  (Supplementary 22  
 Fig. S14). We found that in the presence of magnesium, there was 23  
 a marked decrease in the spring constant of the virion, as previously 24  
 observed for phage  $\lambda$ <sup>27</sup>. This result shows that either magnesium 25  
 ions condense the genome, and thereby reduce the forces that 26  
 drive the genome in close contact with the inner capsid wall, or 27  
 that magnesium ions screen the interaction between capsid and 28  
 genome. The presence of densely packed RNA explains how both 29  
 the virion and the alkaline-triggered uncoating intermediate have 30

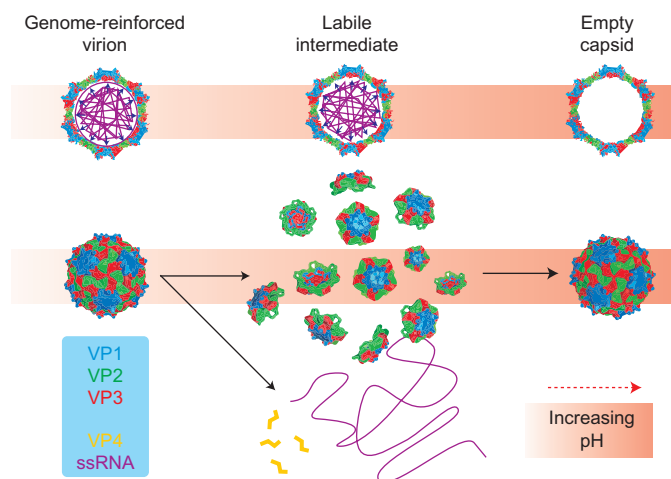


**Figure 4 | Schematic of the alkaline-triggered uncoating of TrV.** Under neutral pH, TrV confines a very large genome. This comes at a high energetic cost, but the ssRNA stabilizes the capsid and thereby prevents premature uncoating. At higher pH, this stabilizing interaction is lost and electrostatic self-repulsion of the ssRNA increases because of the loss of charge on counterions; the capsid bursts and falls apart into pentons. The genome and VP4 are released into the solution and pentons reassemble into empty capsids.

type 2 (ref. 36). Thus, the mechanism of uncoating for TrV is probably distinct from that for picornaviruses. Given the infection route of TrV, it seems only logical that the virus should be acid stable. TrV infects its host through an oral–faecal route<sup>21</sup>. It passes the acidic crop (stomach) of the insect before it reaches the mid- and hindgut, where it enters and infects cells<sup>37</sup>. The gut of the insect reaches a higher pH on feeding, which suggests that timing of the virus release from infected cells is required<sup>17,20</sup>. The acid stability of the virion thus prevents premature uncoating. Non-enveloped ssRNA viruses do not typically encounter alkaline conditions during cell entry. However, the alkaline conditions (up to pH 8.9) reached in the intestinal tract of the insect may induce a softened, labile state of TrV that is required for effective infection. The requirement of a softened state for successful infection has been shown for retroviral particles<sup>38</sup>.

The genome size of picorna and picorna-like viruses is typically in the range 7–10 kb. The observation that the capsid of TrV has to accommodate an enormous amount of ssRNA has important implications for the assembly and stability of the virion. Recently, it was shown that mutations towards a bipartite genome in foot-and-mouth disease virus confer an enhanced stability to the virion and increase fitness<sup>32</sup>. Genome size is thus limiting to viral replication because of the unfavourable state of confining a large negatively charged polymer in a small volume. This barrier will also have to be overcome during genome packaging. The pathway of virion assembly is largely unknown for picorna(-like) viruses. Simple coassembly of ssRNA and pentons will not be energetically feasible and requires condensation of the genome on counterions. Our results show that the packaging capacity of viral capsids is related directly to the stability of the loaded particle, which suggests that the use of viruses as nanocontainers is limited not only by the packaging volume but also by capsid–cargo interactions and destabilizing effects of heavy loads.

In summary, the combination of native MS and AFM allowed us to study uncoating comprehensively in terms of the biophysical properties of TrV. Our current model for the mechanism of uncoating is defined uniquely by an intermediate state uncovered using AFM by virtue of the single-molecule approach. However, this state could only be defined as intermediate to empty capsids because native MS showed that it still contained the ssRNA. Conversely, native MS uncovered the pathway of uncoating via reversible disassembly of the virion, and a topology model of the assembly intermediate was confirmed by AFM. This report shows how native MS and AFM are highly complementary tools for the structural and biophysical characterization of viruses, which enabled us to discover a novel *in vitro* uncoating pathway for dicistroviruses.

## Methods

**TrV purification.** TrV was purified from *T. infestans* faeces using protocols described previously<sup>14</sup>.

**Mass spectrometry.** Samples were buffer exchanged to 150–200 mM ammonium acetate at the indicated pH and a final concentration of 5–10  $\mu$ M (based on the heterotrimer). A 1–2  $\mu$ l aliquot was loaded into gold-coated capillaries for nanoelectrospray ionization (nESI). Capillaries for nESI were home-made from borosilicate glass tubes of 1.2 mm outer diameter and 0.68 mm inner diameter (World Precision Instruments) using a P-97 micropipette puller (Sutter Instruments) and gold-coated using an Edwards Scancoat (Edwards Laboratories) six Pirani 501 sputter coater. MS was performed on modified QToF I and QToF II instruments (Waters, and MS Vision)<sup>39</sup>. Spectra were mass calibrated with caesium iodide. Capillary voltage was in the range 1,300–1,500V, and the sample cone 120–200 V. To optimize transmission of larger ions, the backing pressure was elevated to  $\sim 10$  mbar<sup>40</sup>. Xenon was used as collision gas at a pressure of  $1\text{--}2 \times 10^{-2}$  mbar<sup>41</sup>.

IMS was performed on a Synapt G1 instrument (Waters)<sup>42</sup>. Source conditions were as described above. Xenon was used as the collision gas and nitrogen as the buffer gas in the TWIMS (trans-membrane water and ion measurement system) cell. For analysis of the penton and decamer complexes, as well as of the corresponding globular protein standards, IMS was performed using a ramped wave height of 2–

1 higher breaking forces than those of empty capsids. When applying  
2 forces to the shells, the enclosed RNA will resist actual indentation  
3 and instead the capsid deforms into an oblate sphere (maximizing  
4 the inner volume to accommodate the RNA). It was shown in molec-  
5 ular dynamics simulations of AFM nanoindentation experiments  
6 of similarly sized particles that irreversible distortion is dominated  
7 by locally imposed curvature<sup>34</sup>. The maximum imposed  
8 curvature will be smaller for deformation into oblate spheres than  
9 in true indentation, which explains the high breaking forces of the  
10 virion and uncoating intermediate compared with those of  
11 empty capsids.

## Discussion

13 The data from our AFM and MS experiments suggest the following  
14 model for alkaline-triggered uncoating in TrV. Under neutral con-  
15 ditions, the large genome stabilizes the capsid. As the pH rises,  
16 the genome–capsid interactions are lost and the condensing  
17 strength of counterions decreases, but the genome is still contained.  
18 This leads to a labile shell at the very limit of its packaging capacity.  
19 On further increases in pH, this labile intermediate is unable to  
20 resist the electrostatic and entropic forces that drive the genome out-  
21 wards, and it eventually bursts and disassembles into pentons of  
22  $5 \times \text{VP1}/2/3$ . The genome and VP4 are released into solution and  
23 pentons reassemble into empty capsids. A schematic overview of  
24 the model is presented in Fig. 4. Alternatively, the genome and  
25 VP4 may be expelled from an otherwise intact capsid, as observed  
26 for poliovirus<sup>35</sup>. This does not, however, account for the presence  
27 of pentons during the uncoating reaction. Also, the absence of  
28 pentons from samples of n-empty capsids deems it unlikely that  
29 pentons arise from a penton–capsid equilibrium that is initiated  
30 on genome release.

31 Whether the observed pathway of alkaline-triggered uncoating is  
32 representative of uncoating *in vivo* remains unresolved, as most  
33 aspects of genome release are still unknown for picorna(-like)  
34 viruses. The acid stability of TrV excludes low endosomal pH as a  
35 sufficient trigger for uncoating; other factors are thus required.  
36 Also, it was recently shown that empty TrV capsids produced by  
37 heating a virion sample do not display any morphological changes  
38 similar to those described for either poliovirus or human rhinovirus

- 12 V, ramped over 60% of the cycle. The nitrogen gas pressure in the TWIMS cell was  $5.55 \times 10^{-1}$  mbar. Cross-sections were calibrated based on known cross-sections of denatured ubiquitin, cytochrome c and myoglobin ( $5 \mu\text{M}$  in 50/45/5 water/acetonitrile/formic acid) and native GroEL ( $5 \mu\text{M}$  in 75 mM ammonium acetate pH 6.8)<sup>26,43</sup>. *In silico* cross-section calculations were performed with MobCal, which gave similar results to the Driftscope projection approximation algorithm<sup>44,45</sup>.
- Owing to their size, collisional cross-section values for TrV virions and capsids had to be calibrated using native GroEL (as above) with hepatitis B virus (HBV) capsids as standards<sup>46</sup>. The integrity of the calibrants under the conditions used was verified by calibration of HBV data with GroEL and comparison with previously published results. Measurements were performed at 1.35 kV capillary and 150 V cone voltages with 6 mbar backing pressure. Additional settings were as follows: 50 V in the trap, 75 V in the transfer, both at  $2.3 \times 10^{-2}$  mbar xenon with 500  $\mu\text{s}$  trap-release time; 70 V over the IMS cell running at 250  $\text{m s}^{-1}$  wave velocity and 15–30 V full-cycle wave-height ramping at  $4.6 \times 10^{-1}$  mbar nitrogen.
- AFM.** Virus samples were analysed in 200 mM ammonium acetate at the indicated pH. Silanized glass slides were used as the substrate for AFM. Glass slides were prepared as described previously<sup>47</sup>. Briefly, after thorough rinsing with MilliQ water, the slides were incubated overnight in an ethanol/water (90/10%) bath saturated with potassium hydroxide. After another round of rinsing in MilliQ water, the glass slides were dried and incubated overnight in a hexamethyldisilazane vapour. A 100  $\mu\text{l}$  droplet of virus solution was incubated on the silanized substrate for exactly 30 minutes before adding another 100  $\mu\text{l}$  of ammonium acetate buffer, wetting the AFM tip and mounting the head on the sample. We used Olympus OMCL-RC800PSA silicon nitride cantilevers with a nominal spring constant of 0.05  $\text{N m}^{-1}$  and nominal tip radius of 15 nm. Cantilevers were calibrated using the method of Sader *et al.*<sup>48</sup> to give an average value of  $0.056 \pm 0.006 \text{ N m}^{-1}$ . Imaging and nanoindentation were performed on a Nanotec Electronica AFM operated in jumping mode. The average maximum imaging force was  $\sim 50$  pN. Nanoindentation was performed at a probe velocity of  $\sim 60 \text{ nm s}^{-1}$  and data were processed using a home-built Labview application<sup>49</sup>. Image processing was performed using WSxM software<sup>50</sup>.
- Biochemical analysis and binding energy calculations.** Experimental procedures for native PAGE and autofluorescence analysis of TrV, as well as the procedure used to calculate the binding energies, are given in the Supplementary Information.
- Received 3 October 2012; accepted 15 March 2012;  
published online XX XX 2013
- ## References
- Speir, J. A. & Johnson, J. E. Nucleic acid packaging in viruses. *Curr. Opin. Struct. Biol.* **22**, 65–71 (2012).
  - Douglas, T. & Young, M. Viruses: making friends with old foes. *Science* **312**, 873–875 (2006).
  - Mateu, M. G. Mechanical properties of viruses analyzed by atomic force microscopy: a virological perspective. *Virus Res.* **168**, 1–22 (2012).
  - Morton, V. L., Stockley, P. G., Stonehouse, N. J. & Ashcroft, A. E. Insights into virus capsid assembly from non-covalent mass spectrometry. *Mass Spectrom. Rev.* **27**, 575–595 (2008).
  - Roos, W. H., Bruinsma, R. & Wuite, G. J. L. Physical virology. *Nature Phys.* **6**, 733–743 (2010).
  - Utrecht, C. & Heck, A. J. R. Modern biomolecular mass spectrometry and its role in studying virus structure, dynamics, and assembly. *Angew. Chem. Int. Ed.* **50**, 8248–8262 (2011).
  - Utrecht, C., Barbu, I. M., Shoemaker, G. K., Van Duijn, E. & Heck, A. J. R. Interrogating viral capsid assembly with ion mobility mass spectrometry. *Nature Chem.* **3**, 126–132 (2011).
  - Bonning, B. C. & Miller, W. A. Dicitroviruses. *Ann. Rev. Entomol.* **55**, 129–150 (2010).
  - Marti, G. A. *et al.* Prevalence and distribution of parasites and pathogens of *Triatominae* from Argentina, with emphasis on *Triatoma infestans* and *Triatoma virus* TrV. *J. Invertebr. Pathol.* **102**, 233–237 (2009).
  - Muscio, O. A., La Torre, J. L., Bonder, M. A. & Scodeller, E. A. *Triatoma virus* pathogenicity in laboratory colonies of *Triatoma infestans* (Hemiptera: Reduviidae). *J. Med. Entomol.* **34**, 253–256 (1997).
  - Rassi, A. Jr, Rassi, A. & Marin-Neto, J. A. Chagas disease. *Lancet* **375**, 1388–1402 (2010).
  - Muscio, O. A., La Torre, J. L. & Scodeller, E. A. Characterization of *Triatoma virus*, a picorna-like virus isolated from the triatomine bug *Triatoma infestans*. *J. Gen. Virol.* **69**, 2929–2934 (1988).
  - Czibener, C., La Torre, J. L., Muscio, O. A., Ugalde, R. A. & Scodeller, E. A. Nucleotide sequence analysis of *Triatoma virus* shows that it is a member of a novel group of insect RNA viruses. *J. Gen. Virol.* **81**, 1149–1154 (2000).
  - Agirre, J. *et al.* Capsid protein identification and analysis of mature *Triatoma virus* (TrV) virions and naturally occurring empty particles. *Virology* **409**, 91–101 (2011).
  - Tate, J. *et al.* The crystal structure of cricket paralysis virus: the first view of a new virus family. *Nature Struct. Biol.* **6**, 765–774 (1999).
  - Kumar, S. & Bandyopadhyay, U. Free heme toxicity and its detoxification systems in human. *Toxicol. Lett.* **157**, 175–188 (2005).
  - Schaub, G. A. in *Advances in Insect Physiology* (eds Simpson, S. J. and Casas, J.) Ch. 4, 177–242 (Academic Press, 2009).
  - Oliveira, M. F. *et al.* Heme crystallization in the midgut of triatomine insects. *Comp. Biochem. Physiol. C* **146**, 168–174 (2007).
  - Stiebler, R. *et al.* On the physico-chemical and physiological requirements of hemozoin formation promoted by perimicrovillar membranes in *Rhodnius prolixus* midgut. *Insect Biochem. Mol. Biol.* **40**, 284–292 (2010).
  - Kollien, A. H., Grospietsch, T., Kleffmann, T., Zerbst-Boroffka, I. & Schaub, G. A. Ionic composition of the rectal contents and excreta of the reduviid bug *Triatoma infestans*. *J. Insect Physiol.* **47**, 739–747 (2001).
  - Muscio, O., Bonder, M. A., La Torre, J. L. & Scodeller, E. A. Horizontal transmission of *Triatoma virus* through the fecal–oral route in *Triatoma infestans* (Hemiptera: Triatomidae). *J. Med. Entomol.* **37**, 271–275 (2000).
  - Li, C., Wang, J. C., Taylor, M. W. & Zlotnick, A. *In vitro* assembly of an empty picornavirus capsid follows a dodecahedral path. *J. Virol.* **86**, 13062–13069 (2012).
  - Benesch, J. L. P. Collisional activation of protein complexes: picking up the pieces. *J. Am. Soc. Mass Spectrom.* **20**, 341–348 (2009).
  - Benesch, J. L. P., Ruotolo, B. T., Simmons, D. A. & Robinsons, C. V. Protein complexes in the gas phase: technology for structural genomics and proteomics. *Chem. Rev.* **107**, 3544–3567 (2007).
  - Utrecht, C., Rose, R. J., Van Duijn, E., Lorenzen, K. & Heck, A. J. R. Ion mobility mass spectrometry of proteins and protein assemblies. *Chem. Soc. Rev.* **39**, 1633–1655 (2010).
  - Ruotolo, B. T., Benesch, J. L. P., Sandercock, A. M., Hyung, S. & Robinson, C. V. Ion mobility mass spectrometry analysis of large protein complexes. *Nature Protocols* **3**, 1139–1152 (2008).
  - Evilevitch, A. *et al.* Effects of salts on internal DNA pressure and mechanical properties of phage capsids. *J. Mol. Biol.* **405**, 18–23 (2011).
  - Carrasco, C. *et al.* DNA-mediated anisotropic mechanical reinforcement of a virus. *Proc. Natl Acad. Sci. USA* **103**, 13706–13711 (2006).
  - Michel, J. P. *et al.* Nanoindentation studies of full and empty viral capsids and the effects of capsid protein mutations on elasticity and strength. *Proc. Natl Acad. Sci. USA* **103**, 6184–6189 (2006).
  - Estrozi, L. F. *et al.* Phasing of the *Triatoma virus* diffraction data using a cryo-electron microscopy reconstruction. *Virology* **375**, 85–93 (2008).
  - Castellanos, M., Pérez, R., Carrillo, P. J. P., De Pablo, P. J. & Mateu, M. G. Mechanical disassembly of single virus particles reveals kinetic intermediates predicted by theory. *Biophys. J.* **102**, 2615–2624 (2012).
  - Ojosnegros, S. *et al.* Viral genome segmentation can result from a trade-off between genetic content and particle stability. *PLoS Genetics* **7**, e1001344 (2011).
  - Fout, G. S., Medappa, K. C., Mapoles, J. E. & Rueckert, R. R. Radiochemical determination of polyamines in poliovirus and human rhinovirus 14. *J. Biol. Chem.* **259**, 3639–3643 (1984).
  - Roos, W. H. *et al.* Squeezing protein shells: how continuum elastic models, molecular dynamics simulations, and experiments coalesce at the nanoscale. *Biophys. J.* **99**, 1175–1181 (2010).
  - Bostina, M., Levy, H., Filman, D. J. & Hogle, J. M. Poliovirus RNA is released from the capsid near a twofold symmetry axis. *J. Virol.* **85**, 776–783 (2011).
  - Agirre, J. *et al.* Cryo-TEM reconstructions of *Triatoma virus* particles: a clue to unravel genome delivery and capsid disassembly. *J. Gen. Virol.* <http://dx.doi.org/10.1099/vir.0.048553-0> (2013).
  - Muscio, O. A., La Torre, J. L. & Scodeller, E. A. Small nonoccluded viruses from triatomine bug *Triatoma infestans* (Hemiptera: Reduviidae). *J. Invertebr. Pathol.* **49**, 218–220 (1987).
  - Kol, N. *et al.* A stiffness switch in human immunodeficiency virus. *Biophys. J.* **92**, 1777–1783 (2007).
  - Van Den Heuvel, R. H. H. *et al.* Improving the performance of a quadrupole time-of-flight instrument for macromolecular mass spectrometry. *Anal. Chem.* **78**, 7473–7483 (2006).
  - Tahallah, N., Pinks, M., Maier, C. S. & Heck, A. J. R. The effect of the source pressure on the abundance of ions of noncovalent protein assemblies in an electrospray ionization orthogonal time-of-flight instrument. *Rapid Commun. Mass Spectrom.* **15**, 596–601 (2001).
  - Lorenzen, K., Versluis, C., van Duijn, E., van den Heuvel, R. H. H. & Heck, A. J. R. Optimizing macromolecular tandem mass spectrometry of large non-covalent complexes using heavy collision gases. *Int. J. Mass Spectrom.* **268**, 198–206 (2007).
  - Pringle, S. D. *et al.* An investigation of the mobility separation of some peptide and protein ions using a new hybrid quadrupole/travelling wave IMS/oa-ToF instrument. *Int. J. Mass Spectrom.* **261**, 1–12 (2007).
  - Bush, M. F. *et al.* Collision cross sections of proteins and their complexes: a calibration framework and database for gas-phase structural biology. *Anal. Chem.* **82**, 9557–9565 (2010).

- 1 44. Mesleh, M. F., Hunter, J. M., Shvartsburg, A. A., Schatz, G. C. & Jarrold, M. F.  
2 Structural information from ion mobility measurements: effects of the long-  
3 range potential. *J. Phys. Chem.* **100**, 16082–16086 (1996).
- 4 45. Shvartsburg, A. A. & Jarrold, M. F. An exact hard-spheres scattering model for  
5 the mobilities of polyatomic ions. *Chem. Phys. Lett.* **261**, 86–91 (1996).
- 6 46. Utrecht, C. *et al.* Stability and shape of hepatitis B virus capsids *in vacuo*.  
7 *Angew. Chem. Int. Ed.* **47**, 6247–6251 (2008).
- 8 47. Roos, W. H. How to perform a nanoindentation experiment on a virus. *Methods*  
9 *Mol. Biol.* **783**, 251–264 (2011).
- 10 48. Sader, J. E., Chon, J. W. M. & Mulvaney, P. Calibration of rectangular atomic  
11 force microscope cantilevers. *Rev. Sci. Instrum.* **70**, 3967–3969 (1999).
- 12 49. Snijder, J., Ivanovska, I. L., Baclayon, M., Roos, W. H. & Wuite, G. J. L. Probing  
13 the impact of loading rate on the mechanical properties of viral nanoparticles.  
14 *Micron* **43**, 1343–1350 (2012).
- 15 50. Horcas, I. *et al.* WSXM: a software for scanning probe microscopy and a tool for  
16 nanotechnology. *Rev. Sci. Instrum.* **78**, 013705 (2007).
- 17 **Acknowledgements**
- 18 G.J.L.W. is supported by a NanoSci-E+ grant from FOM (Fundamenteel Onderzoekder  
19 Materie) under the 'Physics of the Genome' program and by a Vici grant from the  
20 Netherlands Organization for Scientific Research (NWO). J.S., C.U., R.J.R. and A.J.R.H. are  
21 supported by the Netherlands Proteomics Centre. A.J.R.H. is further supported by NWO  
22 under ALW-ECHO (819.02.10). R.S-E. is recipient of a predoctoral fellowship from the  
Basque Government (BG). G.A.M. is supported partially by PICT 2008-0035 and V188  
(National University of La Plata). D.M.A.G. is supported by CYTED (Programa  
Internacional de Cooperación Científica y Tecnológica Multilateral) (209RT0364), by the  
BG (MV-2012-2-41; AE-2012-1-44, SPE1 1FB001) and by the Ministry of Science and  
Innovation (BFU2007-62062). We thank the Scientific Calculation Service of the  
UPV/EHU (SGIker) for computation resources.
- 23  
24  
25  
26  
27  
28
- Author contributions**
- A.J.R.H., W.H.R., J.S. and D.M.A.G. conceptually conceived the research. G.A.M., J.A. and  
R.S-E. purified the virus samples. J.S., C.U., R.J.R. and A.J.R.H. performed and supervised  
the MS measurements. J.S. and W.H.R. performed and supervised the AFM measurements.  
R.S.E. and J.A. performed additional experiments. All authors contributed to interpreting  
the data and writing the paper. D.M.G., G.J.L.W. and A.J.R.H. supervised the work in the  
respective laboratories.
- 29  
30  
31  
32  
33  
34  
35
- Additional information**
- Supplementary information is available in the online version of the paper. Reprints and  
permissions information is available online at [www.nature.com/reprints](http://www.nature.com/reprints). Correspondence and  
requests for materials should be addressed to A.J.R.H. and W.H.R.
- 36  
37  
38  
39
- Competing financial interests**
- The authors declare no competing financial interests.
- 40  
41

**PUBLISHER:** Nature  
**PAPER NO.** NCHEM-1627  
**AUTHORS:** Dr Wouter Roos  
**PAPER TITLE:** Probing the biophysical interplay between a viral genome and its capsid

**Author queries**

<b>AUTHOR MANUSCRIPT PAGE</b>	<b>NO.</b>	<b>QUERIES</b>	<b>REPLY</b>
Second paragraph, second sentence	1	This was unclear, so I have reworded it slightly, OK? If not, please amend as necessary.	
Figure 3d caption, first sentence	2	This was a little unclear in the original (was two sentences), so I have reworded it slightly, OK? If not, please amend as necessary.	